

A Model for the Offsets between X-ray and Radio Emission from Large Scale AGN Jets

M. G. Kim^{1*} and F. Takahara¹

¹*Department of Earth and Space Science, Graduate School of Science, Osaka University, Toyonaka, Osaka 560-0043, Japan*

ABSTRACT

We investigate apparent internal structure of kiloparsec scale jets of AGNs arising from the energy dependent cooling of accelerated electrons and light travel time effect for relativistically moving sources. Using a simple cylindrical shell model, we find that the offsets between the peaks of X-ray, optical and radio brightness distributions observed for many cases are basically explained with this model. Assuming that electrons in the moving shell are instantaneously accelerated, X-rays are emitted for a shorter time scale and observed at the side nearer to the nucleus, while radio emission continues to the far side of the nucleus because of longer cooling time. The resultant offset turns out to be order of the jet diameter owing to the light travel time effect.

Key words: galaxies: active – galaxies: jets – radiation mechanisms: non-thermal – X-rays: galaxies

1 INTRODUCTION

It is well known that kiloparsec scale jets of radio loud AGNs consist of many bright knots seen in X-ray and optical in addition to the radio bands. For this decade the *Chandra X-Ray Observatory* has detected large scale jets for tens of objects with a sub-arcsecond resolution. Combining with radio and optical observations with similar spatial resolution, offsets between different observation bands have been noticed, e.g., for M87 (Marshall et al. 2002; Wilson & Yang 2002), Cen A (Kraft et al. 2002; Hardcastle et al. 2003), PKS 1127-145 (Siemiginowska et al. 2002), 3C 66B (Hardcastle, Birkinshaw & Worrall 2001) and 3C 31 (Hardcastle et al. 2002). It is intriguing that almost always the centroids of X-ray knots are located closer to the core than those of lower frequencies. In M87 (Wilson & Yang 2002; Marshall et al. 2002), the centroids of optical knots are closer to the core than their radio counterparts (for a recent review, see Harris & Krawczynski (2006)). While the emission mechanism of radio through optical emission is believed to be synchrotron radiation by relativistic electrons, several mechanisms are proposed for X-ray emission. X-rays from the knots of FR I galaxies such as M87, Cen A, 3C 66B and 3C 31 are well interpreted with synchrotron radiation by multi-TeV energy electrons, while for quasars such as PKS 1127-145 the mechanism has not been settled yet. It may be inverse Compton scattering of CMB photons by lower energy electrons with the aid of strong relativistic beaming effect even on this large scale (Siemiginowska et al. 2002, 2007).

In this paper, assuming that X-ray emission is synchrotron radiation by high energy electrons we discuss the origin of the observed offsets and address the question why in all cases, knots at higher frequencies are located closer to the core than their counterparts at lower frequencies. Bai & Lee (2003) suggested that time lags due to synchrotron losses can make these X-ray/optical and X-ray/radio offsets. In the shock acceleration scenario, electrons in large scale jets can be accelerated to energies high enough to emit synchrotron X-rays. As they propagate downstream along the jet, electrons cool as they emit at progressively lower frequencies and result in radio/X-ray offsets at bright knots, e.g., the centroids of X-ray knots should be observed closer to the core. In this case, however, we expect to see a time delay from high to low frequencies if cooling effect is the sole cause of the offsets. It is also noted that cooling time of radio emitting electrons is too long to explain the observed offset. In reality, X-ray/radio offsets are seen at the same time for distant observers and electron acceleration occurs for a finite time span and over a finite spatial extent. Therefore, light travel time effects should be taken into account, too.

This paper examines the possibility that X-ray/radio offsets can be explained by a single shock wave that accelerates electrons for a finite time span, by considering the energy dependent cooling timescale of relativistic electrons and light travel time effect of a relativistically moving source with a finite spatial extent. In §2, we describe these effects and our model, §3 and §4 present the results and discussion, respectively. Finally, §5 summarizes our conclusions.

* E-mail: mgkim@vega.ess.sci.osaka-u.ac.jp

2 THE MODEL

2.1 Light travel time effect

The light travel time effect is relevant when we consider relativistically moving sources which have a finite spatial extent, for example when a shock wave, or any kind of inhomogeneities, travels along the jet. In such cases, emission from different positions in the jet at the same coordinate time reaches the observer at different time and will produce changes in the apparent shape of the brightness distribution as viewed from the observer. In other words, the apparent shape seen by the observer is different from the shape of the emission region at the same coordinate time. The difference is dependent on the viewing angle and the jet speed.

First, we explain the simplest case shown in Fig. 1, i.e., an infinitesimally thin rectilinear rod moving at a velocity of β , normalized by the speed of light c , viewed at a viewing angle θ . The emission region has a finite length from the point A to B. Let the point D be located at the distance ℓ from the point A. The difference of arrival times at the observer between the radiation emitted from point A at the time t_0 and that from point D at the time $t_0 + \Delta t$ is expressed as

$$\Delta t_{\text{obs}} = \Delta t - \left(\frac{\ell}{c} + \beta \Delta t \right) \cos \theta. \quad (1)$$

The condition of the same observer time $\Delta t_{\text{obs}} = 0$ gives the time difference of emission between the points A and D as

$$\Delta t = \frac{\ell \cos \theta}{c(1 - \beta \cos \theta)}. \quad (2)$$

When the relativistic beaming effect is significant ($\cos \theta \approx \beta$), the time difference Δt becomes larger than ℓ/c about by a factor of $\Gamma^2 = 1/(1 - \beta^2)$. Moreover, the apparent distance between points A and D, ℓ_{obs} , is

$$\ell_{\text{obs}} = (\ell + \beta c \Delta t) \sin \theta = \frac{\ell \sin \theta}{1 - \beta \cos \theta}. \quad (3)$$

This is also significantly larger than ℓ for relativistically beamed sources. It is noted that this effect is also important for unbeamed sources as far as the cooling time scale is shorter than Δt in equation (2). Interpretation of the jet structure should take into account this light travel time effect. In reality the thickness of the jet should be taken into account as is described in §2.3.

2.2 Effects of radiative cooling of high energy electrons

Another important aspect is the effect of the finite cooling time of relativistic electrons. It is widely accepted that electrons are accelerated by shocks in the jet. In the framework of diffusive shock acceleration (Blandford & Eichler 1987; Bell 1978), the time needed to accelerate electrons to a Lorentz factor γ in the jet comoving frame is (Inoue & Takahara 1996; Kusunose, Takahara & Li 2000)

$$t_{\text{acc}}(\gamma) = \frac{20\lambda(\gamma)c}{3u_s^2} \sim \xi \left(\frac{\gamma}{10^7} \right) \left(\frac{B}{1\text{G}} \right)^{-1} \text{sec}, \quad (4)$$

where $u_s \sim c$ is the shock speed, B is the magnetic field strength, $\lambda(\gamma) = \xi \gamma m_e c^2 / (eB)$ is the mean free path of electrons assumed to be proportional to the electron Larmor

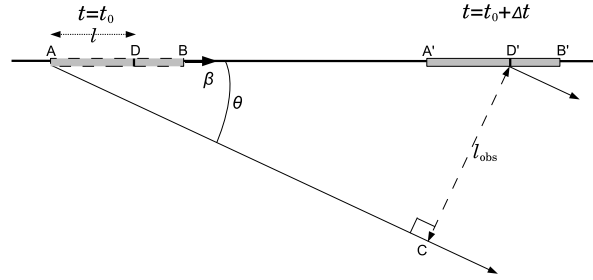


Figure 1. The light travel time effect for the radiation emitted from an infinitesimally thin rectilinear rod moving at a velocity of β viewed at a viewing angle θ . The emission region has a finite length from the point A to B. The difference of arrival times at the observer between the radiation emitted from point A at time t_0 and that from point D at the time $t_0 + \Delta t$, represented as D' , is different from Δt .

radius with ξ being a parameter ($\xi \geq 1$ and $\xi = 1$ corresponds to the Böhm limit), m_e is the electron mass, and $-e$ is the electron charge. This equation implies that only several thousand seconds are needed to accelerate electrons to the energy for which electrons emit synchrotron X-ray radiation in 1 mG magnetic field. The radiative cooling time $t_{\text{cool}}(\gamma)$ of relativistic electrons through synchrotron radiation is

$$t_{\text{cool}}(\gamma) = \frac{3m_e c}{4\sigma_T} U_B^{-1} \gamma^{-1}, \quad (5)$$

where σ_T is the Thomson cross section and $U_B = B^2/(8\pi)$ is the energy density of the magnetic field.

In the jet comoving frame, the typical synchrotron emission frequency of relativistic electrons, averaged over pitch angle, is

$$\nu_s = \frac{3}{4} \nu_B \gamma^2 = \frac{3e}{8\pi m_e c} B \gamma^2 \quad (6)$$

where $\nu_B = eB/(2\pi m_e c)$ is Larmor frequency. In terms of ν_s , equation (5) can be expressed as

$$t_{\text{cool}} \simeq 2\delta^{1/2} \left(\frac{B}{1\text{mG}} \right)^{-3/2} \left(\frac{\nu_{\text{obs}}}{10^{17}\text{Hz}} \right)^{-1/2} \text{yr} \quad (7)$$

where $\nu_{\text{obs}} = \delta \nu_s$ is the typical synchrotron frequency in the observer frame and $\delta = [\Gamma(1 - \beta \cos \theta)]^{-1}$ is the Doppler factor. For example, the cooling time of high energy electrons emitting 10^{17}Hz photons and that of low energy ones emitting 1GHz photons, differs by four orders of magnitude. Thus, high energy electrons tend to be spatially confined near the shock front, while low energy electrons tend to be distributed in a more extended region.

2.3 The model

To investigate the above two effects, as the simplest model we consider the emission from a shell with radius R and width W moving at a constant bulk Lorentz factor Γ and investigate the brightness distribution in the sky plane observed far from the jet with a viewing angle θ . Hereafter, we adopt the cylindrical coordinate (r, ϕ, z) with z -axis being the direction of the bulk motion as shown in Fig. 2. Let us consider the time delay between two points A and B in

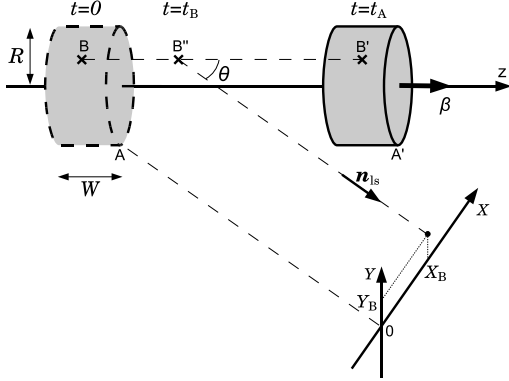


Figure 2. The emission from a shell with radius R and width W moving at a constant velocity β and the brightness distribution in the sky plane observed far from the jet with a viewing angle θ . The shell begins to emit radiation at $t = 0$ and moves till $t = t_A$ along the z -axis. The point A represents the nearest position of the shell along the line of sight, while the point B represents an arbitrary position in the shell. The radiation emitted from the point B in the shell at the time $t = t_B$ (the position designated by B'') is observed at (X_B, Y_B) in the sky X-Y plane which is set transverse to the line of sight. The origin $(X, Y) = (0, 0)$ is the position where the radiation emitted from the position A at $t = 0$ is observed.

the shell, the coordinates of which at time $t = 0$ are given by (r_A, ϕ_A, z_A) and (r_B, ϕ_B, z_B) , respectively. The point A represents the nearest position of the shell along the line of sight, while the point B represents an arbitrary position in the shell. We assume that at $t = 0$ the shell begins to emit radiation and that the emission continues till $t = t_{\text{cool}}$. In this case, the time delay between the radiation emitted from the point B in the shell at the time $t = t_B$ (the position designated by B'') and the radiation emitted from the point A in the shell at the time $t = t_A$ (the position designated by A') is

$$\Delta t_{\text{obs}} = (t_A - t_B) + \mathbf{D} \cdot \mathbf{n}_{\text{ls}}/c, \quad (8)$$

where $\mathbf{D} \equiv \overrightarrow{A'B''}$ is the vector connecting the positions $A'(r_A, \phi_A, c\beta t_A + z_A)$ and $B''(r_B, \phi_B, c\beta t_B + z_B)$ and \mathbf{n}_{ls} is the unit vector toward the observer along the line of sight. For definition of the plane of sky, we set the sky plane coordinates transverse to the line of sight as (X, Y) and set the unit vectors as $\mathbf{n}_X \equiv (\mathbf{n}_z - (\mathbf{n}_z \cdot \mathbf{n}_{\text{ls}})\mathbf{n}_{\text{ls}})/|\mathbf{n}_z - (\mathbf{n}_z \cdot \mathbf{n}_{\text{ls}})\mathbf{n}_{\text{ls}}|$ and $\mathbf{n}_Y \equiv \mathbf{n}_{\text{ls}} \times \mathbf{n}_X/|\mathbf{n}_{\text{ls}} \times \mathbf{n}_X|$, where \mathbf{n}_z is the unit vector along the z -axis. The origin $(X, Y) = (0, 0)$ on the X-Y plane is taken as the position where the radiation emitted from the point A at $t = 0$ is observed. The point B'' is observed at (X_B, Y_B) , where

$$X_B = (\mathbf{D} + c\beta t_B \mathbf{n}_z) \cdot \mathbf{n}_X \quad (9)$$

$$Y_B = (\mathbf{D} + c\beta t_B \mathbf{n}_z) \cdot \mathbf{n}_Y \quad (10)$$

By calculating equations (9) and (10) under the condition $\Delta t_{\text{obs}} = 0$, we determine the position and time of the point B'' which is observed simultaneously with the point A'. Considering the coordinates of point B take a range of $0 \leq r_B \leq r_A, 0 \leq \phi_B \leq 2\pi, 0 \leq z_B \leq z_A$, the brightness distribution on the plane of sky can be calculated.

In this paper, in order to demonstrate the effects of energy dependent radiative cooling we consider the simplest case where electrons have only two different energies. Lower energy electrons have longer cooling time $t_{\text{cool,low}}$ and higher energy electrons shorter one $t_{\text{cool,high}}$. Moreover, we treat $t_{\text{cool,low}}$ and $t_{\text{cool,high}}$ as phenomenological parameters and simply assume that electrons radiate at a constant rate for the respective time spans.

As for the particle acceleration, we ignore the acceleration timescale and assume that electrons of all energy begin to emit synchrotron radiation at the same time $t = 0$, because the acceleration timescale is much shorter than the cooling timescales.

Of course, this model is just a toy model to demonstrate effects of light travel time and energy dependent radiative cooling. To improve on more realistic cases is not difficult once these effects are understood.

2.4 Analysis in the $Y = \text{const.}$ plane

Owing to the energy dependent cooling, an offset between the brightness distributions of high and low frequency emission arises when the light travel time and cooling effects are taken into account. Here, we discuss the typical magnitude expected in the two-dimensional plane containing the vector \mathbf{n}_{ls} and \mathbf{n}_z , as seen in Fig. 3. In the sky plane, this plane is projected onto the line of $Y = \text{const.}$ We set the x -axis transverse to the z -axis to describe the position of the shell material and generalize the consideration made in section 2.1 to the shell with a finite thickness. Since $\mathbf{n}_{\text{ls}} = (\sin \theta, \cos \theta)$ and $\mathbf{D} = (x_B - x_A, z_B - z_A + c\beta(t_B - t_A))$, using equation (8) the condition of simultaneous observation $\Delta t_{\text{obs}} = 0$ gives the difference of the emission time for the points A and B, $\Delta t = t_A - t_B$, as

$$\Delta t = \frac{\Delta x \sin \theta + \Delta z \cos \theta}{c(1 - \beta \cos \theta)} \quad (11)$$

where $\Delta x = x_A - x_B$ and $\Delta z = z_A - z_B$. So the maximum value of Δt is expressed as

$$\text{Max}(\Delta t) = \frac{2R \sin \theta + W \cos \theta}{c(1 - \beta \cos \theta)}. \quad (12)$$

The position and time of the point B''($x_{B''}, z_{B''}$) observed simultaneously with point A' at $t = t_A$ are given respectively by using the relation $z_{B''} = z_B + c\beta t_B$ and $x_{B''} = x_B$ as

$$z_{B''} = \frac{(x_B - x_A)\beta \sin \theta + z_B - z_A \beta \cos \theta}{1 - \beta \cos \theta} + c\beta t_A \quad (13)$$

and

$$t_B = \frac{(x_B - x_A) \sin \theta}{c} + \frac{(z_{B''} - z_A) \cos \theta}{c} + t_A(1 - \beta \cos \theta). \quad (14)$$

The coordinates of x_B and z_B take a range of $-R \leq x_B \leq R = x_A$ and $0 \leq z_B \leq W = z_A$, so the region observed simultaneously can be drawn by equation (13) as the grey-colored region in Fig. 3 for a given value of t_A . In Fig. 3, the radiating shell moves along the z -axis (from left to right) and both light and dark grey-colored regions represent the regions observed simultaneously. The region is segmented by a range of source time t_B such that for more distant part along the line of sight the source time is earlier. The dark grey-colored region represents the region of high frequency

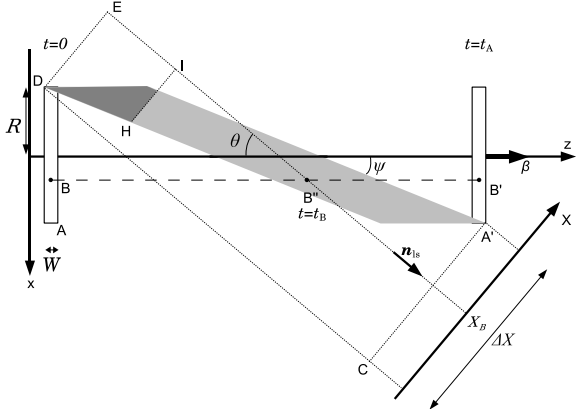


Figure 3. The observable region of a moving shell in the two-dimensional plane containing the vector \mathbf{n}_s and \mathbf{n}_z . We set the x -axis transverse to the z -axis. The radiating shell moves along the z -axis from left to right and both light and dark grey-colored regions represent the region observed simultaneously. The region is segmented by a range of source time such that for more distant part along the line of sight the emission time is earlier. The dark grey-colored region represents the region of high frequency radiation, while the light grey-colored region represents the region of low frequency radiation.

radiation, while the light grey-colored region represents the region of low frequency radiation. It should be noted that in Fig. 3 we assume that the particle acceleration occurs instantaneously $t = 0$ and synchrotron radiation begins at the time $t = 0$, and we set the time $t_A = \text{Max}(\Delta t)$ and the cooling timescales satisfy $t_{\text{cool,high}} < t_A < t_{\text{cool,low}}$.

The lines DE , HI and CA' in Fig. 3 represent those of equal source time $t = 0$, $t_{\text{cool,high}}$ and t_A , respectively. So both the light and dark grey regions are observable at the low frequency while at the high frequency only the dark grey region is observed.

Because we assume that the emissivity in the shell is independent of time as far as $t \leq t_{\text{cool}}$, the brightness on the plane of sky is simply proportional to the length of the emitting region along the line of sight. Then we can calculate the brightness distribution along the X -axis and see the offset between the brightness distributions between the high and low frequencies.

The inclination of the hatched region is given by

$$\tan \psi = \frac{1 - \beta \cos \theta}{\beta \sin \theta}, \quad (15)$$

so that $\theta > \psi$ when $\sin \theta > 1/\Gamma$ and $\theta < \psi$ when $\sin \theta < 1/\Gamma$. Fig. 3 depicts the former case and the apparent size of the shell seen in the low frequency is given by

$$\Delta X = \frac{2R |\beta - \cos \theta| + W \sin \theta}{1 - \beta \cos \theta}. \quad (16)$$

For the latter case, it is also given by equation (16). We notice the apparent size gives the upper limit on the offset.

3 RESULTS

Here we present the brightness distribution on the plane of sky at two frequencies corresponding to two energies of elec-

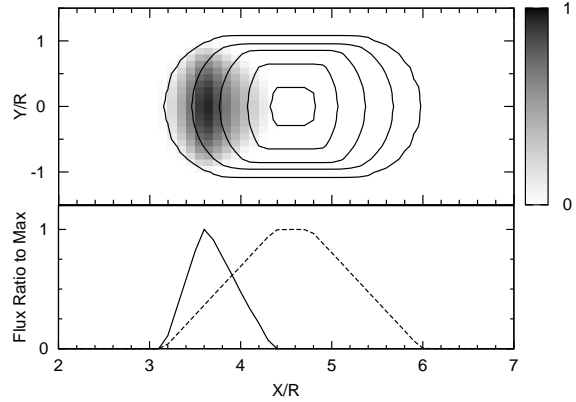


Figure 4. Top panel: The brightness contour of the radiation emitted from the shell which is observed at the observer time $t_{\text{obs}} \simeq 0.75R/c$. The X and Y axes are the same as in Fig. 2. We set $t_A = 30R/c$, $\sin \theta = 2/\Gamma$, $t_{\text{cool,low}} = 60R/c$, $t_{\text{cool,high}} = 0.2t_{\text{cool,low}}$, $W/R = 0.2$ and $\Gamma = 10$. The solid line contours show the brightness distribution from the low energy electrons, while the gray-colored contour shows that from the high energy ones. The line contours represent from outside to inside 2%, 25%, 50%, 75%, and 95% of the peak value. The density of the gray contour shows the ratio of the brightness to its peak value. Bottom: The brightness distribution along the $Y = 0$ axis in the top panel. The solid line shows the high energy flux and broken line does the low energy one. The magnitude of the offset between the peaks of two distributions is $D_{\text{off}} \sim 1.0R$.

trons. Especially, the cases that the viewing angle is around $1/\Gamma$ are investigated.

Fig. 4 shows the brightness contour of the synchrotron radiation emitted from the shell which is observed at the observer time $t_{\text{obs}} \simeq 0.75R/c$ where we set the source time $t_A = 30R/c$, viewing angle $\sin \theta = 2/\Gamma$, cooling times $t_{\text{cool,low}} = 60R/c$, $t_{\text{cool,high}} = 0.2t_{\text{cool,low}} = 12R/c$, the ratio $W/R = 0.2$ and bulk Lorentz factor $\Gamma = 10$. By equation (1) we set the observer time $t_{\text{obs}} = t_A(1 - \beta \cos \theta)$ and $t_{\text{obs}} = 0$ represent the time when the emission from the point A at $t = 0$ is observed. The solid line contours show the brightness distribution from the low energy electrons, while the gray-colored contour shows that from the high energy ones. The line contours represent 2%, 25%, 50%, 75%, and 95% of the peak value from outside to inside. The density of the gray contour shows the ratio of the brightness to its peak value. Obviously, the offset between the centroid of the line contours and that of the gray-colored region is seen. The magnitude of the offset turns out to be $D_{\text{off}} \sim 1.0R$ for this case.

The offset is not due to the beaming effect (Rybicki & Lightman 1979) but the relativistic motion of jet. That is shown in Fig. 5 where the velocity of jet is the same as that in Fig. 4 but the viewing angle is much larger than $1/\Gamma$. Fig. 5 shows the brightness contours at the observer time $t_{\text{obs}} \simeq 4.3R/c$ for the case of $t_A = 21R/c$, $\sin \theta = 4/\Gamma$, $t_{\text{cool,low}} = 60R/c$, $t_{\text{cool,high}} = 0.2t_{\text{cool,low}} = 12R/c$, $\Gamma = 10$ and $W/R = 0.2$. In this case, the offset turns out to be $D_{\text{off}} \sim 0.9R$ and almost the same as that in Fig. 4.

The magnitude of the offset is dependent on the assumed parameters. Fig. 6 shows the brightness contours at

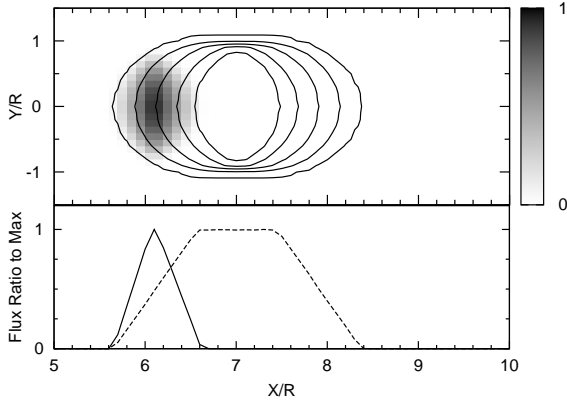


Figure 5. Top panel: The brightness contour which is observed at the observer time $t_{\text{obs}} \simeq 4.3R/c$. We set $t_A = 21R/c$, $\sin \theta = 4/\Gamma$, $t_{\text{cool,low}} = 60R/c$, $t_{\text{cool,high}} = 0.2t_{\text{cool,low}}$, $W/R = 0.2$ and $\Gamma = 10$. Bottom: The brightness distribution along the $Y = 0$ axis in the top panel. The magnitude of the offset between the peaks of two distributions is $D_{\text{off}} \sim 0.9R$.

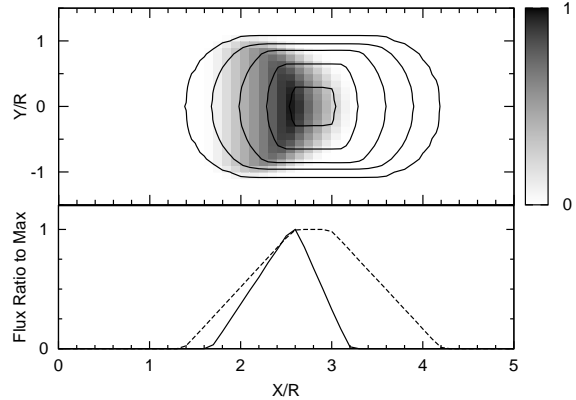


Figure 6. Top panel: The brightness contour which is observed at the observer time $t_{\text{obs}} \simeq 0.3R/c$. We set $t_A = 48R/c$, $\sin \theta = 1/(2\Gamma)$, $t_{\text{cool,low}} = 60R/c$, $t_{\text{cool,high}} = 0.2t_{\text{cool,low}}$, $W/R = 0.2$ and $\Gamma = 10$. Bottom: The brightness distribution along the $Y = 0$ axis in the top panel. The peak of the high energy radiation is located inside of the region where the brightness of the low energy radiation has a flat top peak, but has an offset $D_{\text{off}} \sim 0.2R$.

the observer time $t_{\text{obs}} \simeq 0.3R/c$ for the case of $t_A = 48R/c$, $\sin \theta = 1/(2\Gamma)$, $t_{\text{cool,low}} = 60R/c$, $t_{\text{cool,high}} = 0.2t_{\text{cool,low}} = 12R/c$, $\Gamma = 10$ and $W/R = 0.2$. In this case, the offset turns out to be $D_{\text{off}} \sim 0.2R$. The difference is largely due to the difference in viewing angle. As has been noted in the previous section, the case $\sin \theta = 2/\Gamma$ the shell is seen from the tail side while for $\sin \theta = 1/(2\Gamma)$ it is seen from the front side. As is seen in Figs. 4 and 6 larger offset is expected when $\sin \theta > 1/\Gamma$, while the offset is small when $\sin \theta < 1/\Gamma$. Fig. 7 describes a closer inspection of the situation. As is seen in the former case, the brightness peak from the high energy electrons (the position designated by X_{high} is located outside the flat top peak of the brightness contour from the low energy ones (the segment designated by $X_{\alpha}X_{\beta}$), while for the latter case the position X_{high} is inside the segment $X_{\alpha}X_{\beta}$. For the both cases, it is noticed the offset between the position X_{high} and X_{low} , which represent the centroid of the brightness distribution from the low energy ones, exist.

The brightness profile is also time-dependent. In Fig. 8, the time variation of the brightness distribution on the plane of sky is shown for the case shown in Fig. 4. The profiles of line contours and greyscale contours are shown in the same way as in Fig. 4, and all the brightness distributions are normalized by the peak values for each epoch. The epoch for panels (a) ~ (e) is $t_{\text{obs}}/(R/c) = 0.3, 0.45, 0.53, 0.75$ and 0.9 corresponding to $t_A/(R/c) = 12, 18, 21, 30$ and 36 , respectively. As is seen in panels (a) and (b), the offset is not significant for early stage before higher energy electrons cool. After high energy electrons have cooled, the offset arises and becomes larger with time as seen in panels (c) ~ (e). As a result, while the high energy radiation is observed for a time span of $0.90R/c$, offset is observed from $0.53R/c$ to $0.9R/c$. Thus, the offset is observed for about a half of the observing time of the high energy flux. Moreover, the area covering the low frequency emission keeps increasing, but that of the high frequency emission first increases and reaches a maximum in panel (b) and turns to decrease afterward. This time variation may be one of the reasons why the extent of the offsets is different in different knots, including the cases of

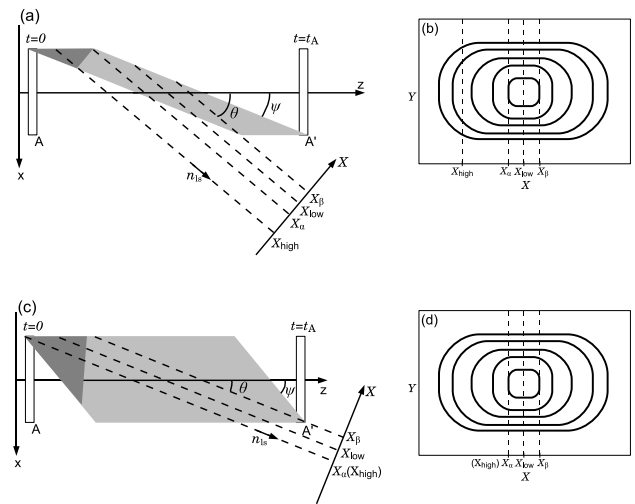


Figure 7. The difference between the cases of $\sin \theta > 1/\Gamma$ and $\sin \theta < 1/\Gamma$. The upper panels are for $\sin \theta > 1/\Gamma$, while the lower panels are for $\sin \theta < 1/\Gamma$. The left panels show the moving shell in the two-dimensional plane and both light and dark grey-colored regions represent the region observed simultaneously as in Fig. 3 and the segmentation is also the same as in Fig. 3. The right panels show the brightness contours of the low energy radiation. In both panels, the centroid of the high energy radiation is marked by $X = X_{\text{high}}$ while that of the low energy one is by $X = X_{\text{low}}$. The brightness of the low energy radiation shows a flat top distribution between $X = X_{\alpha}$ and X_{β} .

no offset. After some time the shell emits only emission from lower energy electrons and seen only in the radio band.

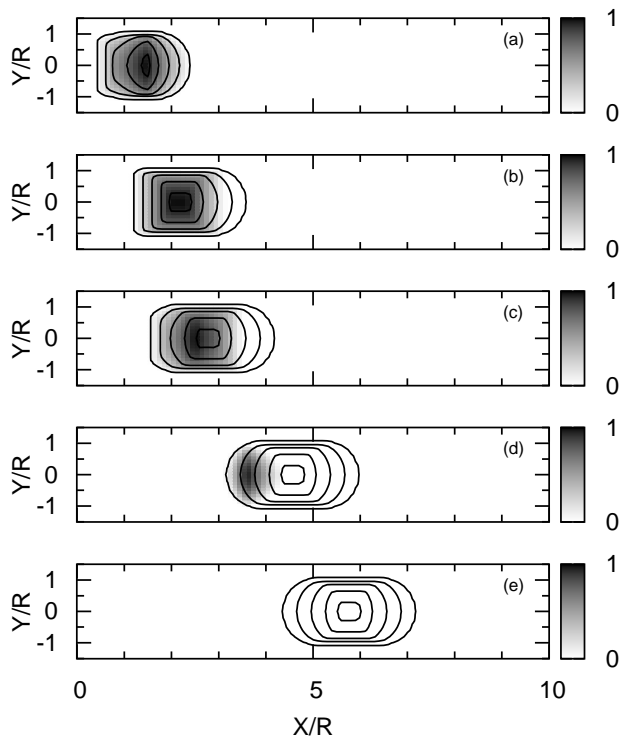


Figure 8. Time evolution of the brightness distribution on the plane of sky for the case shown in Fig. 4. The profiles of line and greyscale contours are depicted in the same way as in Fig. 4, and all the brightness distributions are normalized by the peak value for each epoch. The epoch for panel (a) \sim (e) corresponds to $t_{\text{obs}}/(R/c) = 0.3, 0.45, 0.53, 0.75$ and 0.9 , respectively.

4 DISCUSSION

4.1 Statistics of the offsets

We have shown that the offset between X-rays and radio emission naturally arises when we take account of the energy dependent radiative cooling of relativistic electrons and the light travel time effect for moving sources. We estimated that roughly half of the X-ray knots should show an offset from the radio knots.

In the above we adopted an artificially large ratio of the cooling time of X-ray emitting electrons to that of radio emitting electrons as 0.2 compared with the realistic value of around 10^{-4} . This does not affect the above conclusion but affect the fraction in which X-ray knots are observed among radio knots. In the above we have assumed that particle acceleration is instantaneous but in reality particle acceleration occurs for a finite time span. The observability of X-ray knots is determined by the ratio of this time span to the cooling time of radio emitting electrons. In addition, adiabatic expansion of radio knots may play a role in determining the life time of radio knots.

The ratio of the cooling time of radio emitting to the maximum time difference of emission time in the source $\text{Max}(\Delta t)$ is given by

$$\frac{t_{\text{cool,low}}}{\text{Max}(\Delta t)} = \left(\frac{R}{6 \times 10^3 \text{pc}} \right)^{-1} \left(\frac{B}{1 \text{mG}} \right)^{-3/2} \left(\frac{\nu_{\text{obs}}}{1 \text{GHz}} \right)^{-1/2}$$

$$\times \left(\frac{1 - \beta \cos \theta}{2 \sin \theta + (W/R) \cos \theta} \right) \delta^{1/2}. \quad (17)$$

The order of magnitude of this value is of order unity, which is compatible with our model.

4.2 Implication for the individual offsets in M87 and Cen A

Now we discuss on the application of our model to the offsets seen in typical objects. First, we discuss on FRI radio galaxies such as M 87 and Cen A. Although for FRI radio galaxies viewing angle is relatively large and relativistic beaming effects are mild, the offset between X-ray and radio emission is expected as far as the knots are moving relativistically or even at mildly relativistic velocities. And its magnitude is a significant fraction of ΔX . As for M87 located at a distance of 16 Mpc and $1'' = 78 \text{pc}$, the observed radio/X-ray offsets are found as $0''.5$ for knot D and $0''.7$ for knot F (Wilson & Yang 2002), while ΔX in our model is estimated as $2''.0$ for $\theta = 20^\circ$, $\Gamma = 10$ (Biretta, Sparks & Macchetto 1999), $R = 58.5 \text{pc}$ corresponding to $0''.75$ and $W/R = 0.2$. For $B = 10^{-4} G$ (Wilson & Yang 2002) and R satisfies equation (17) which means high energy electrons cool sufficiently fast. It is interesting to note that the X-ray knots D and F are not separated from the radio knots but a part of the radio knots, which is fully consistent with our results shown in Figs. 4 and 6. Thus, our model is compatible with observations of M87.

In Cen A located at a distance of 3.4 Mpc and $1'' = 17 \text{pc}$, the radio/X-ray offsets increase from $1''.3$ for knots A2A/AX2 to $3''$ for knots A3B/AX3A and $8''$ for B1A/BX2 (Hardcastle et al. 2003). This feature is probably due to the increase of the jet radius R with the distance from the nucleus and we set $R = 2'', 3'', 14''$ (Kraft et al. 2002) for respective knots corresponding to $R = 34 \text{pc}, 51 \text{pc}$ and 238pc . These radii satisfies the cooling condition of equation (17). It should be noticed the viewing angle and velocity of the jet in Cen A are not well determined only with the constraints of $50^\circ < \theta < 80^\circ$ and $\beta > 0.45$ (Tingay et al. 1998; Jones et al. 1996). Thus, we examine two sets of parameters. First we set a large viewing angle and relativistic velocity such as $\theta = 80^\circ$, $\Gamma = 10$, $B = 10^{-4} G$ and $W/R = 0.2$. For this set we obtain ΔX of $4''.4, 6''.7, 31''$ for respective knots. (The differences of ΔX come from those of R .) Second choice is a moderate viewing angle and moderate velocity such as $\theta = 50^\circ$, $\Gamma = 1.1$, $B = 10^{-4} G$ and $W/R = 0.2$. For this case we obtain ΔX of $1''.0, 1''.6, 7''.2$ for respective knots and these are smaller than the observations. Thus, the first case of larger viewing angle and faster velocity of jet are preferred.

Finally, we discuss on offsets of quasar jet in PKS 1127-145 which located at $z = 1.187$ and $1''$ corresponds to 11.5kpc (Stanghellini et al. 1998). The largescale radio/X-ray offsets are found as $2''.1$ for knot A, $1''.4$ for knot B and $0''.8$ for knot C (Siemiginowska et al. 2002). The jet radius R is around $2''$ for every knots (Siemiginowska et al. 2002) and satisfies equation (17) for $B = 1 \text{mG}$. However, the viewing angle and velocity of the jet are not well known yet (Siemiginowska et al. 2002, 2007) so we examine parameters which meet the condition $\Delta X > 2''$ by equation (16). Consequently we find when $\Gamma > 5$ or $\sin \theta < 0.7/\Gamma$ or $\sin \theta > 1.3/\Gamma$ the magnitudes of the offsets are compatible with our model.

However, X-ray emission mechanism in these sources is still an open problem because the X-ray spectrum is definitely flatter than the extrapolation of radio to optical spectrum (Siemiginowska et al. 2002). In spite of this complexities, the offset may suggest that X-rays are from high energy electrons with short cooling time.

5 SUMMARY

We investigated apparent internal structure of kiloparsec scale jets of AGNs arising from the energy dependent cooling of accelerated electrons and light travel time effect for relativistically moving sources. Using a simple cylindrical shell model, we find that the offsets between the peaks of X-ray, optical and radio brightness distributions observed for many cases are basically explained. Assuming that electrons in the moving shell are instantaneously accelerated, X-rays are emitted for a shorter time scale and observed at the side nearer to the nucleus, while radio emission continues to the far side of the nucleus because of longer cooling time. The resultant offset in Fig. 4 turns out to be order of the jet diameter owing to the light travel time effect.

The magnitude of the offset is dependent on the viewing angle θ and differs by one order of magnitude when $\sin\theta$ varies from $2/\Gamma$ to $1/(2\Gamma)$. We showed that the appearance of the offset alters at $\sin\theta = 1/\Gamma$ as shown in Fig. 7. When $\sin\theta > 1/\Gamma$ we see the shell from the tail side, while when $\sin\theta < 1/\Gamma$ we see it from the front side.

We also investigated the time evolution of the brightness profile. The offset is not significant for early stage before higher energy electrons cool. After the stage when high energy electrons have cooled, the offset arises and becomes larger with time. As a result, the offset is observed for about a half of the observing time of the X-ray knots. This time variation may be one of the reasons why the extent of the offsets is different in different knots, including the cases of no offset.

Finally we argued that the observed offsets in FR I radio galaxies M87 and Cen A and other kpc jets of quasar PKS 1127-145 are well interpreted with our model.

REFERENCES

- Bai J. M., Lee M. G., 2003, ApJ, 585, 113
 Bell A. R., 1978, MNRAS, 182, 147
 Biretta J. A., Sparks W. B., Macchetto F., 1999, ApJ, 520, 621
 Blandford R. D., Eichler D., 1987, Phys.Rep., 154, 1
 Ghisellini G., Celotti A., Fossati G., Maraschi L., Comastri A., 1998, MNRAS, 301, 451
 Hardcastle M. J., Birkinshaw M., Worrall D. M., 2001, MNRAS, 326, 1499
 Hardcastle M. J., Worrall D. M., Birkinshaw M., Laing R. A., Brindle A. H., 2002, MNRAS, 334, 184
 Hardcastle M. J., Worrall D. M., Kraft R. P., Forman W. R., Jones C., Murray S. S., 2003, ApJ, 593, 169
 Harris D. E., Krawczynski H., 2002, ApJ, 565, 244
 Harris D. E., Krawczynski H., 2006, ARA&A, 44, 463
 Inoue S., Takahara F., 1996, ApJ, 463, 555
 Jones D. L. et al., 1996, ApJ, 466, L63
 Kraft R. P., Forman W. R., Jones D., Murray S. S., Hardcastle M. J., Worrall K. M., 2002, ApJ, 569, 54
 Kusunose M., Takahara F., Li, H., 2000, ApJ, 536, 299
 Marshall H. L., Miller B. P., Davis D. S., Perlman E. S., Wise M., Danizares D. R., Harris D. E., 2002, ApJ, 564, 683
 Rybicki, G.B., Lightman, A., 1979, Radiative Processes in Astrophysics, New York, Wiley
 Siemiginowska A., Bechtold J., Aldcroft T. L., Elvis M., Harris D. E. Dobrzycki A., 2002, ApJ, 570, 543
 Siemiginowska A., Stawrz L., Cheung C. C., Harris D. E., Sikora M., Aldcroft T. L., Bechtold J., 2007, ApJ, 657, 145
 Stanghellini C., O’Dea C. P., Dallacasa D., Baum S. A., Fanti R., Fanti C., 1998, A&AS, 131, 303
 Tingay S. J. et al., 1998, ApJ, 115, 960
 Wilson A. S., Yang Y., 2002, ApJ, 568, 133